Metal–Organic Frameworks

Nanoporous Materials Can Tune the Critical Point of a Pure Substance

Efrem Braun, Joseph J. Chen, Sondre K. Schnell, Li-Chiang Lin, Jeffrey A. Reimer,* and Berend Smit*

Abstract: Molecular simulations and NMR relaxometry experiments demonstrate that pure benzene or xylene confined in isoreticular metal–organic frameworks (IRMOFs) exhibit true vapor–liquid phase equilibria where the effective critical point may be reduced by tuning the structure of the MOF. Our results are consistent with vapor and liquid phases extending over many MOF unit cells. These results are counterintuitive since the MOF pore diameters are approximately the same length scale as the adsorbate molecules. As applications of these materials in catalysis, separations, and gas storage rely on the ability to tune the properties of adsorbed molecules, we anticipate that the ability to systematically control the critical point, thereby preparing spatially inhomogeneous local adsorbate densities, could add a new design tool for MOF applications.

There is a rich emerging literature on metal-organic frameworks owing to the ability to tune local chemical structure and geometry by joining various metal-containing units with a panoply of organic linkers to create nanoporous crystalline materials.[1] Judicious choice of linker-metal combinations yields MOFs exhibiting ultrahigh porosity in combination with thermal and chemical stability. These are widely explored for applications ranging from separations, storage, catalysis, etc.[2]

Confinement of molecules within pores affects their collective properties, such as phase behavior. A well-known example is capillary condensation[3] where interactions between adsorbed molecules and the pore wall induce quasi one-dimensional vapor-liquid coexistence at conditions where the bulk fluid is singularly present as a vapor. In the literature, capillary condensation is often associated with a single pore, and if the dimensions of this pore are of similar size as the adsorbed molecules, capillary condensation is suppressed; thus, the adsorbed fluid is present as a single phase at all conditions. As the pores of most MOFs are on the order of nanometers, capillary condensation will not occur.

Phase transitions induced by adsorption have been observed in MOFs and are associated with mechanisms other than capillary condensation. For example, in flexible MOFs such as MIL-53 adsorption-induced phase transitions are observed in the host MOF crystals.[4] Other phase transitions observed in nanoporous materials are governed by commensurate-incommensurate transitions in the geometric packing of the molecules in the pores.[5] Our work is motivated by the surprising behavior of benzene and related molecules in IRMOF-1 (MOF-5). Previous NMR and molecular dynamics studies[6] of benzene motion in IRMOF-1 yielded diffusivities associated with two domains of differing mobilities. Adsorption experiments showed features suggesting multiple surface energies.[7] Finally, grand-canonical Monte Carlo simulations[8] detailed a narrow hysteresis loop for cyclohexane in IRMOF-1, which was reluctantly associated with capillary condensation even though the authors noted that the pores of IRMOF-1 are too small to support the effect.[3] In contrast, others proposed that the step in the CO_2 adsorption isotherm in IRMOF-1 is related to a vapor–liquid transition.[9] Other studies, however, do not observe the hysteresis and conclude that attractive electrostatic interactions between CO_2 molecules are responsible for the unusual shape of the adsorption isotherms,[10] or explain such unusual behavior in terms of clustering.[11]

To resolve these differences we used molecular simulations (SI Simulation Methods) to examine the adsorption of benzene and xylenes in a representative set of IRMOFs as shown in Figure 1. Figure 2 illustrates the key result of our Monte Carlo simulations: ordinary vapor–liquid coexistence of benzene in these materials. We observe liquid and vapor phases that are similar to bulk phase coexistence that extend over many unit cells. Figure 3 shows the corresponding phase diagram; the densities indicated by the phase envelope are

[*] E. Braun,[+] Dr. J. J. Chen,[+] Dr. S. K. Schnell, Dr. L.-C. Lin,
Dr. J. A. Reimer, Dr. B. Smit
Department of Chemical and Biomolecular Engineering
University of California, Berkeley
Berkeley, CA 94720 (USA)
E-mail: reimer@berkeley.edu
berend-smit@berkeley.edu

Dr. S. K. Schnell
Department of Chemistry, Norwegian University of Science and
Technology, 7491 Trondheim (Norway)

Dr. L.-C. Lin
Department of Process and Energy, Delft University of Technology
Leeghwaterstraat 39, 2628 CB Delft (The Netherlands)

Dr. J. A. Reimer, Dr. B. Smit
Materials Science Division, Lawrence Berkeley National Laboratory
1 Cyclotron Road, Berkeley, CA 94720 (USA)

Dr. B. Smit
Department of Chemistry, University of California, Berkeley
Berkeley, CA 94720 (USA)

Dr. B. Smit
Institut des Sciences et Ingénierie Chimiques (ISIC), Valais
Ecole Polytechnique Fédérale de Lausanne (EPFL)
Rue de l'Industrie 17, CH-1951 Sion (Switzerland)

[+] These authors contributed equally to this work.

Supporting information and ORCID(s) from the author(s) for this
article are available on the WWW under http://dx.doi.org/10.1002/
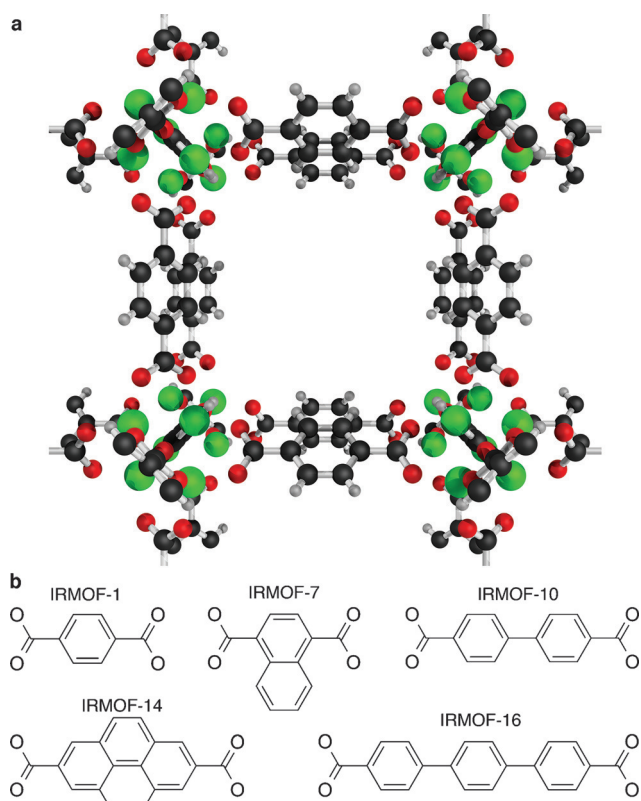anie.201506865.

a

b

Figure 1. a) Crystal structure of IRMOF-1, which consists of Zn$_4$O complexes connected by 1,4-benzene dicarboxylate linkers. b) Linker molecules of all IRMOFs used in the molecular simulations.
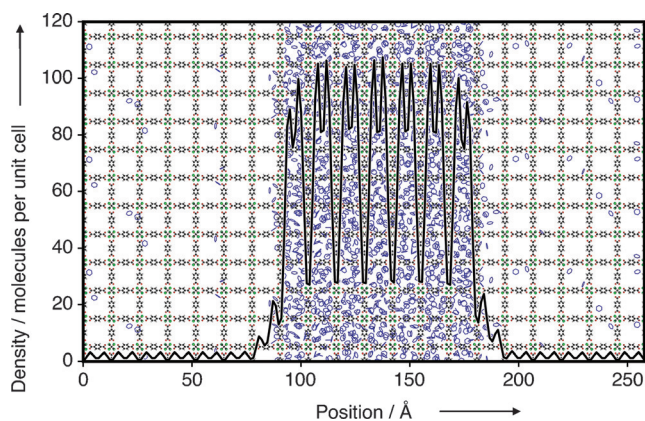

Figure 2. Overlay of the density profile of benzene molecules in IRMOF-1 at 270 K with a snapshot of the system as obtained from NVT Monte Carlo simulations; the snapshot has been scaled to exactly match the density profile's axes. The distribution of this density profile between the two different types of cages present in IRMOF-1 is shown in SI Figure 6. Because of the periodic boundary conditions we observe an infinite slab with two interfaces. The sizes of the liquid and gas slabs depend on the total size of our simulation cell.

consistent with loadings found from the hysteresis loop portion in the adsorption isotherms as obtained from grand-canonical Monte Carlo simulations (SI Figure 1 in the Supporting Information). These results are consistent with
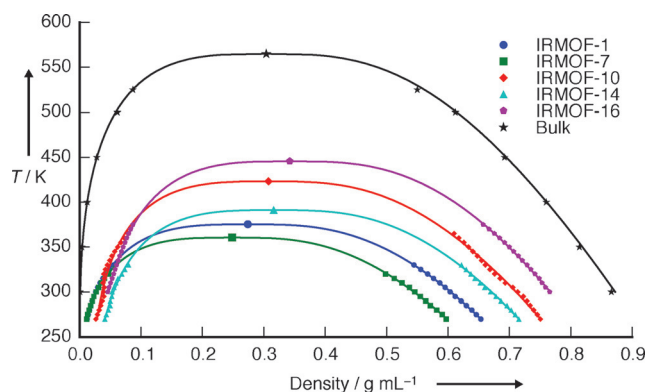

Figure 3. Vapor–liquid coexistence curves for benzene in various IRMOFs. The density scaling law (with the three-dimensional Ising critical exponent $\beta = 0.32$) and the law of rectilinear diameters were used to estimate the critical point and to interpolate the data. Note that the error bars of these calculations are smaller than the symbols. Densities were converted to mass per void space volume using void fractions of 0.832, 0.782, 0.910, 0.914, and 0.939 for IRMOFs 1, 7, 10, 14, and 16, respectively (for details see SI Simulation Methods).

the conclusions reported[9] for CO$_2$ in IRMOF-1. The critical point of benzene in IRMOF-1 was found to be 375 K, about 200 K below the bulk critical point. This decrease in the critical point stems from the frustration of benzene packing in the liquid phase by the ligands of the MOF.

Interestingly, we can leverage the native structural and chemical flexibility afforded by the modular construction of metal-organic frameworks to tune this critical point. Phase diagrams were simulated for benzene in the IRMOF series. We found that as the pore size increases, the critical temperature of benzene increases, approaching its bulk value (Figure 3). For IRMOFs with the same linker length, such as IRMOF-1 and IRMOF-7 or IRMOF-10 and IRMOF-14, the addition of a side group lowers the critical temperature. We surmise that this is because these side groups further frustrate the packing in the liquid phase. Additionally, we repeated our simulations with xylene isomers in IRMOF-1 and found a similar reduction in the critical temperatures for all three isomers (SI Figures 2–5).

Experimental confirmation of vapor–liquid phase transitions lies in the detection of spatially extended domains of vapor–liquid coexistence. Towards that end we turned to NMR relaxometry, a technique that allows us to probe subtle changes in molecular motion. The differing densities of the vapor and liquid phases coexisting within the MOFs are expected to create dissimilar magnetic environments that are distinguishable using NMR spin-spin relaxation measurements. We measured the distribution of spin–spin (T_2) relaxation times using Carr–Purcell–Meiboom–Gill (CPMG)[12] experiments combined with a Laplace inversion numerical analysis algorithm to disentangle the multiple relaxation time constants (SI Experimental Methods).[13]

Figure 4 A illustrates the distribution of T_2 relaxation times obtained from benzene in IRMOF-1 at different temperatures. A single thermodynamic phase of benzene would produce a single relaxation time, yet we observe three separate peaks in the T_2 distributions, illustrating that
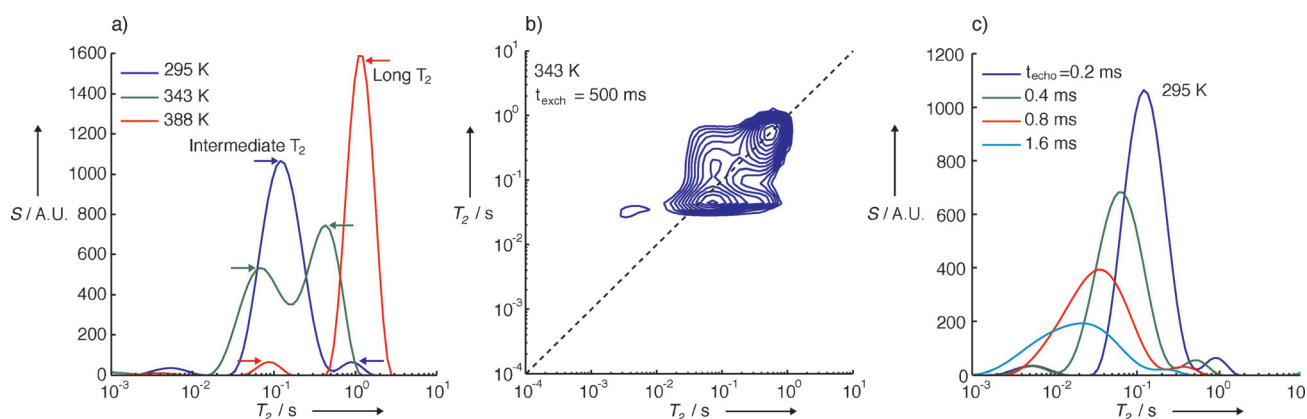
Figure 4. NMR relaxation and exchange of benzene in IRMOF-1. a) T_2 relaxation distributions of benzene in IRMOF-1 at a loading of 9 ± 1 molecules of benzene per unit cell at different temperatures, where the right-facing arrows indicate the intermediate T_2 population and the left-facing arrows indicate the long T_2 population. b) A contour plot of the T_2–T_2 relaxation exchange distribution at 343 K. The off-diagonal intensities illustrate the presence of molecular exchange between the intermediate (liquid) and long (vapor) relaxation time environments during the timescale set by the experiment; in these data $t_{exch} = 500$ ms. c) T_2 relaxation distributions at 295 K with varying echo period (t_{echo}) indicating the presence of magnetic field gradients arising from the vapor–liquid interface.

benzene resides in distinct environments. For example, at 295 K we observe a dominant peak at intermediate relaxation times (≈ 120 ms) as well as a small peak at long relaxation times (≈ 870 ms). We associate the dominant peak with benzene in the liquid phase and the smaller peak with benzene in the vapor phase for two reasons. First, spin–spin relaxation times of adsorbed fluids increase with molecular mobility,[14] hence the shorter T_2 emanates from the liquid phase. Secondly, the experiments are conducted under conditions where the majority of molecules ($\approx 70\%$) reside in the liquid phase. The third small peak (≈ 5 ms) is assigned to molecules near the vapor–liquid interface (SI Discussion). As the temperature increases the peak associated with the liquid phase (intermediate-T_2 relaxation times) decreases in size, corresponding to a decrease in the mole fraction of liquid, while the peak associated with the vapor phase (long-T_2 relaxation times) correspondingly increases in size. This trend continues such that at 343 K the number of molecules associated with each relaxation peak is roughly equal, and at 388 K the vapor phase dominates (SI Discussion). The distinct changes in the peak intensities are convincingly commensurate with the simulated vapor–liquid coexistence curve (Figure 3). Indeed, at higher temperatures more benzene molecules are in the vapor phase.

A unique and defining feature of this coexistence is the extension of the vapor and liquid phases over many unit cells (Figure 2). The corresponding length scales may be probed directly by two-dimensional T_2–T_2 relaxation exchange experiments where the appearance of cross-peaks demonstrates that during the measurement time (t_{exch}) molecules have moved from a liquid phase to a vapor phase. Figure 4 B shows the T_2–T_2 exchange plots for $t_{exch} = 500$ ms when benzene is adsorbed in IRMOF-1. Peaks centered on the diagonal represent benzene molecules that have not exchanged between the liquid and vapor phases during t_{exch}, whereas peaks that are centered symmetrically on either side of the diagonal are associated with molecules that have

exchanged between these phases. Exchange peaks are prominent in Figure 4 B, confirming that the molecules are exchanging between the liquid and vapor phases within a timescale of $t_{exch} = 100$–500 ms (SI Discussion). This time scale, along with a representative diffusion coefficient[6a,b] of benzene in IRMOF-1 ($\approx 10^{-9}$ m^{2}s^{-1}) gives us ca. 10^{-5} m as the characteristic length scale over which a molecule diffuses between both phases. This 10-micron length scale shows that indeed the vapor and liquid phases extend over many unit cells.

A third experimental observation supporting our assignment of two distinct phases is seen in the dependence of spin–spin (T_2) relaxation times on the echo period of the CPMG sequence. An interface such as the one shown in Figure 2 creates spatially-localized magnetic field gradients owing to the differences in magnetic susceptibility (χ) between the vapor and liquid phases.[15] The magnitude of these field gradients increases with proximity to the interface. We directly probe the diffusion of molecules through the vapor–liquid interface by varying the echo period (t_{echo}) in the CPMG experiment.[16] By varying this echo period we tune the window over which we monitor molecular diffusion. With short echo periods, the diffusion length is short, and the effect of the gradient on T_2 is minimal; increasing the echo period increases the effect of the field gradient on T_2. Furthermore, increasing the echo period (and the associated diffusion length) also increases the number of molecules that are influenced by the interface. Both of these effects explain the shortening relaxation times depicted in Figure 4 C.

It is important to distinguish the present phenomenon from capillary condensation. Capillary condensation cannot support a true phase transition in cylindrical pores[3] because the correlation length associated with density fluctuations can only grow in one dimension. Conversely, the IRMOF-type frameworks studied herein exhibit relatively open structures, and hence correlation lengths can grow in any direction, with phase transitions likely belonging to the universal class of the

three-dimensional Ising model.[9] In this context it is interesting to compare these materials to aerogels, which are also open structures and change the vapor–liquid equilibrium curve of adsorbed molecules.[17] In aerogels, however, the porosity is so high that the critical point is only changed by a few mK. The present phenomenon is also distinct from previous reports[11a] of adsorbate clustering in which phase coexistence does not play a role (SI Discussion).

We conclude that even materials with pore sizes on the order of nanometers can support vapor–liquid coexistence provided they possess the correct topology. This provides a natural explanation for the anomalous behavior reported for benzene and related molecules in IRMOF-1.[6,7] More broadly, we anticipate that this phenomenon is not limited to vapor–liquid equilibria. Similar effects, for example, can be expected for liquid-liquid mixtures. The ability to substantially tune the critical point of a pure fluid sheds new light on a very classic phenomenon, portending a revisiting of pure and multicomponent phase behavior in nanoporous materials. The phenomenon of mesoscopic domains of differing adsorbate densities/compositions in MOFs introduces heterogeneity which, similar to multivariate MOFs,[18] has potential applications in catalysis, separations, and storage technologies.

[1] H. Furukawa, K. E. Cordova, M. O'Keeffe, O. M. Yaghi, *Science* **2013**, *341*, 1230444.

[2] A. U. Czaja, N. Trukhan, U. Müller, *Chem. Soc. Rev.* **2009**, *38*, 1284–1293.

[3] L. D. Gelb, K. E. Gubbins, R. Radhkrishnan, M. Sliwinska-Bartkowiak, *Rep. Prog. Phys.* **1999**, *62*, 1573–1659.

[4] a) G. Férey, C. Serre, *Chem. Soc. Rev.* **2009**, *38*, 1380–1399; b) A. Ghysels, L. Vanduyfhuys, M. Vandichel, M. Waroquier, V. Van Speybroeck, B. Smit, *J. Phys. Chem. C* **2013**, *117*, 11540–11554.

[5] B. Smit, T. L. M. Maesen, *Nature* **1995**, *374*, 42–44.

[6] a) F. Stallmach, S. Gröger, V. Künzel, J. Kärger, O. M. Yaghi, M. Hesse, U. Müller, *Angew. Chem. Int. Ed.* **2006**, *45*, 2123–2126; *Angew. Chem.* **2006**, *118*, 2177–2181; b) S. Hertel, M. Wehring, S. Amirjalayer, M. Gratz, J. Lincke, H. Krautscheid, R. Schmid, F. Stallmach, *Eur. Phys. J. Appl. Phys.* **2011**, *55*, 20702; c) D. C. Ford, D. Dubbeldam, R. Q. Snurr, V. Künzel, M. Wehring, F. Stallmach, J. Kärger, U. Muller, *J. Phys. Chem. Lett.* **2012**, *3*, 930–933.

[7] a) W. G. Shim, K. J. Hwang, J. T. Chung, Y. S. Baek, S. J. Yoo, S. C. Kim, H. Moon, J. W. Lee, *Adv. Powder Technol.* **2012**, *23*, 615–619; b) W. Makowski, M. Mańko, P. Zabierowski, K. Mlekodaj, D. Majda, J. Szklarzewicz, W. Łasocha, *Thermochim. Acta* **2014**, *587*, 1–10.

[8] L. Sarkisov, T. Düren, R. Q. Snurr, *Mol. Phys.* **2004**, *102*, 211–221.

[9] M. De Toni, P. Pullumbi, F. X. Coudert, A. H. Fuchs, *J. Phys. Chem. C* **2010**, *114*, 21631–21637.

[10] K. S. Walton, A. R. Millward, D. Dubbeldam, H. Frost, J. J. Low, O. M. Yaghi, R. Q. Snurr, *J. Am. Chem. Soc.* **2008**, *130*, 406–407.

[11] a) R. Krishna, J. M. van Baten, *Langmuir* **2010**, *26*, 3981–3992; b) K. Takakura, T. Ueda, K. Miyakubo, T. Eguchi, *Phys. Chem. Chem. Phys.* **2013**, *15*, 279–290.

[12] a) H. Y. Carr, E. M. Purcell, *Phys. Rev.* **1954**, *94*, 630–638; b) S. Meiboom, D. Gill, *Rev. Sci. Instrum.* **1958**, *29*, 688–691.

[13] L. Venkataramanan, Y. Song, M. D. Hürlimann, *IEEE Trans. Signal Process.* **2002**, *50*, 1017–1026.

[14] Y. Song, *J. Magn. Reson.* **2013**, *229*, 12–24.

[15] V. Vaidyanathan, *Phys. Rev.* **1927**, *30*, 512–515.

[16] a) M. D. Hürlimann, *J. Magn. Reson.* **1998**, *131*, 232–240; b) J. Mitchell, T. C. Chandrasekera, M. L. Johns, L. F. Gladden, E. J. Fordham, *Phys. Rev. E* **2010**, *81*, 026101.

[17] a) A. P. Y. Wong, M. H. W. Chan, *Phys. Rev. Lett.* **1990**, *65*, 2567–2570; b) J. P. Donley, A. J. Liu, *Phys. Rev. E* **1997**, *55*, 539–543.

[18] X. Q. Kong, H. X. Deng, F. Y. Yan, J. Kim, J. A. Swisher, B. Smit, O. M. Yaghi, J. A. Reimer, *Science* **2013**, *341*, 882–885.